https://doi.org/10.5194/egusphere-2023-388
Preprint. Discussion started: 7 March 2023

The evolution of precipitation and warm conveyor belts during the central southwest Asia wet season

Melissa Leah Breeden[1,2], Andrew Hoell[2], John Robert Albers[1,2], and Kimberly Slinski[3,4]

[1]Cooperative Institute for Research in Environmental Sciences, University of Colorado Boulder, Boulder, CO
[2] NOAA Physical Sciences Laboratory, Boulder, CO
[3]NASA Goddard Space Flight Center, Greenbelt, United States
[4]Earth System Science Interdisciplinary Center, University of Maryland, College Park, United States

Correspondence to: Melissa L. Breeden (melissa.breeden@noaa.gov)

Abstract. Understanding the nature of precipitation over central southwest Asia, a data-sparse, semi-arid region, is crucial for anticipating future agricultural productivity and the likelihood of hazards such as flooding. However, the month-to-month evolution of daily precipitation characteristics, such as duration and amplitude, have not been extensively considered. Here we compare how daily precipitation and local vertical motion forcing - represented by warm conveyor belts (WCBs) - evolve from November to April over Afghanistan. Given the low amount of in-situ precipitation observations in the area, we first compare several precipitation estimates, indicating that the seasonal evolution of daily precipitation is consistent across estimates that incorporate satellite information. While these datasets agree on the timing of peak precipitation in February and March, total accumulation amounts vary substantially. Still, a common feature is that the majority of precipitation occurs on the few days when accumulation exceeds 4 mm, which are most frequent in February and March. Precipitation intensity, duration, and the associated circulation patterns evolve as winter progresses into spring, with notable differences within the months from January to April. El Niño conditions are generally associated with more heavy precipitation days than La Niña, consistent with past research, with both enhanced WCB frequency and moisture transport from lower latitudes observed during El Niño conditions, except for in January when neither precipitation nor WCB change. As such, our results support prior connections made between ENSO and seasonal-to-interannual circulation changes and extend this connection to one between the slowly-evolving ENSO influence and transient, synoptic-scale vertical motion represented by WCBs.

1 Introduction

Central southwest Asia (CSWA) includes several food-insecure countries – Afghanistan, Pakistan, Tajikistan and Uzbekistan (FAO, 2022) – that depend heavily on cold season precipitation, as the mountain snowpack and subsequent snowmelt runoff provide a vital source of water for agriculture (Thenkabail et al. 2004; Lotsch et al. 2005; FEWS NET 2018; Qutbudin et al 2019; McNally et al. 2022). Afghanistan in particular receives the vast majority of its precipitation from November – April (Hoell et al. 2015a; Gerlitz et al. 2020), with substantial precipitation generated as flow is forced up the high topography in the central and northeastern portions of the country by westerly cyclonic disturbances (Lang and Barros 2003; Cannon et al. 2017). The area is also prone to flooding, particularly during spring when rain-on-snow events are most

https://doi.org/10.5194/egusphere-2023-388
Preprint. Discussion started: 7 March 2023

common, with substantial impacts to lives and property (Hagen and Teufert 2009). The generally intermittent nature of CSWA precipitation during the cold season produces substantial interannual variability, making the region susceptible to drought, such as the devastating 1999-2001 event that occurred during persistent La Niña conditions (Barlow et al 2002). Given the crucial but unreliable role that precipitation plays in the region, humanitarian food aid is provided to the country by multiple sources including the United States Agency for International Development (USAID), with regularly-issued weather and climate outlooks for Afghanistan provided by the Famine Early Warning Systems Network (FEWS NET; Funk et al. 2019; McNally et al. 2022). The lack of reliable in situ precipitation measurements in the region means that estimating precipitation relies on datasets incorporating satellite-derived quantities (e.g., Funk et al. 2015), and that determining which estimate is 'correct' is not necessarily well-posed. Still, when multiple estimates display agreement, the confidence in the precipitation estimate is enhanced.

Precipitation displays strong variability across timescales from minutes to months (e.g., Trenberth et al. 2017), with large-scale, slowly-evolving phenomena - including the seasonal cycle - modulating, over many regions, the frequency of short-duration, high-amplitude events. Hoell et al. 2015a found that months of anomalously low CSWA precipitation differed from pluvial periods by the presence of equivalent barotropic anticyclonic anomalies located just to the west of Afghanistan, with moisture fluxed southwestward on their eastern flank, also supporting anomalous drying. They demonstrated how different months within the cold season were associated with a variety of combinations of Indo-Pacific sea surface temperature (SST) patterns. It has been well-established that SST variations and the associated tropical convective heating response can modulate CSWA precipitation through the generation of an anomalous Rossby wave source and large-scale vertical motions (Barlow et al. 2002; Hoell et al 2012; Hoell et al. 2013; Hoell et al. 2015b; Hoell et al 2018a; Hoell et al. 2018b). In particular, the El Niño-Southern Oscillation (ENSO) is a strong modulator of southwest Asian climate, with La Niña associated with reduced moisture fluxes (Mariotti et al. 2007) and an anomalous upper-level anticyclone and downward vertical motion (Nazemosadet and Ghasemi 2004; Hoell et al. 2014a; Hoell et al. 2014b; Hoell et al. 2015a; Breeden et al. 2022), both conducive to reduced precipitation that can lead to drought (Barlow et al. 2002). Conversely, anomalous rising motion and enhanced precipitation are observed during El Niño conditions (Hoell et al. 2017).

Past research has focused heavily on CSWA precipitation variability averaged over the November – April wet season or monthly means, consistent with the interest on long-lived precipitation and soil moisture deficits associated with drought. While precipitation in this region is undoubtedly affected by low-frequency climate oscillations, such as ENSO or the seasonal cycle, precipitation ultimately varies on shorter timescales on the order of hours and days, with a small number of intense events contributing an outsize amount to the long-term mean (Pendergrass and Knutti 2018), as has been previously acknowledged to be the case in this region (Hoell et al. 2015a). The link between transient 'westerly disturbances' and CSWA precipitation has been mentioned in prior studies (Barlow et al. 2016; Cannon et al. 2017), but the relationship between precipitation and synoptic features over southwest Asia has not been heavily studied (Barlow et al. 2016), particularly regarding their seasonality. A global study of warm conveyor belts (WCBs), the warm, moist, strongly ascending airstreams associated with extratropical cyclones (e.g., Green et al. 1966; Wernli and Davies 1997; Madonna et al. 2014; Pfahl et al. 2014) did find

https://doi.org/10.5194/egusphere-2023-388
Preprint. Discussion started: 7 March 2023

that a substantial portion of total annual precipitation over CSWA was associated with these features (Pfahl et al. 2014), though the seasonality and circulation patterns associated with WCBs in this region have not been heavily discussed in the present literature. As such, how daily precipitation and WCBs associated with CSWA precipitation evolve during the boreal cold season is the focus of the present analysis.

This study uses daily precipitation from several datasets including satellite-derived, reanalysis, and gauge-based estimates to consider how daily CSWA precipitation evolves within the cold season. First, the datasets were compared to confirm that the seasonal evolution of precipitation was consistent, which was found to be the case for datasets incorporating satellite-derived information. Accumulation peaks from February – April, when vertical motion forcing from transient extratropical cyclones also peaks, although total accumulation values were not found to be consistent among datasets in this region. Furthermore, the circulation patterns that are associated with heavy precipitation events evolves as winter progresses into spring. The frequency of heavy precipitation events is modulated by the phase of ENSO, consistent with past studies linking El Niño (EN) or La Niña (LN) conditions to wet and dry conditions over the region, respectively. The occurrence of heavy precipitation days increases during EN conditions, most notably in March, related to both enhanced moisture fluxes from the Arabian Peninsula and enhanced vertical motion forcing associated with extratropical cyclones.

2. Data and Methodology

2.1 Data

Afghanistan is a data-sparse region (Hoell et al. 2015a; Sun et al. 2018), so first we verify that the precipitation characteristics discussed are not a function of the precipitation dataset chosen, by comparing the statistics of daily mean precipitation from five different products: two reanalysis products, two remote-sensing and gauge-based products, and one solely gauge-based product (Table 1; Figs. 1-2). The longest common period for JRA55, CHIRPS, ERA5 and CPC precipitation is 1981-2020, while the shorter common period of 2001-2019 is also considered to include a comparison with IMERG. CHIRPS and IMERG are combined satellite-gauge products, although relatively few rain gauges are located within Afghanistan, meaning these precipitation estimates are largely satellite-derived. JRA55 and ERA5 precipitation are reanalysis products and are therefore estimates that are physically consistent with other variables in the model. Reanalysis-based precipitation estimates incorporate satellite-derived precipitation estimates, which are spatially inhomogeneous over long periods, with model data used to fill in the spatial and temporal gaps, and are available at relatively short latency (3-5 days for JRA55 and ERA5, respectively), making them amenable to generating near real-time forecasts needed by FEWS NET. As such, knowing how these two reanalysis products compare to alternatively-derived precipitation estimates from CHIRPS and IMERG is considered valuable. Finally, we include the NOAA Climate Prediction Center (CPC) Unified Gauge precipitation dataset to consider the representation of precipitation from a purely gauge-based product. We also emphasize that given the sparsity of in-situ precipitation records over Afghanistan and that the number of stations in the country has historically varied markedly (CHC UCSB 2023), the goal of comparing the datasets is to confirm that the aspects of precipitation considered are consistently observed by reliable products, and less to emphasize which product is the most ‘correct’ regarding exact precipitation amounts.

https://doi.org/10.5194/egusphere-2023-388
Preprint. Discussion started: 7 March 2023

To consider the circulation associated with heavy precipitation events, daily mean ERA5 200- and 750- hPa streamfunction field were accessed at 2.5x2.5° horizontal resolution and daily mean horizontal ERA5 vertically integrated moisture fluxes (IVT) were accessed at .25x.25° horizontal resolution (Hersbach et al. 2020). To track strong upward vertical motion associated specifically with extratropical cyclones, the warm conveyor belt (WCB) frequency dataset (Madonna et al. 2014; Sprenger et al. 2017) was used based on ERA-Interim reanalysis. In this dataset, WCBs are tracked by locating air parcel trajectories within the vicinity of an extratropical cyclone that originate in the lower troposphere and ascend at least 600 hPa within two days. As such, WCB occurrences highlight regions of strong ascent that are associated specifically with low-level cyclones. The frequency of 6-hourly timesteps indicating a WCB were averaged to daily means and is considered at 1x1° horizontal resolution. To partition months by ENSO phase, the Oceanic Niño Index (ONI), which is based on the Niño3.4 index (Trenberth 1997) that averages monthly mean SSTs in the region 5°N-5°S, 170°W-120°W and applies a three-month running mean, was acquired from the CPC (https://origin.cpc.ncep.noaa.gov/products/analysis_monitoring/ensostuff/ONI_v5.php). In section 3, El Niño (EN) conditions are defined when the ONI is at least a value of +0.5°, and La Niña (LN) conditions are defined when the ONI is less than or equal to -0.5°. Events during the period 1981-2017 are considered to be consistent with the precipitation and WCB datasets (CHIRPS begins in 1981, and WCBs are tracked through 2017).

2.2 Precipitation Duration and Intensity

We consider the probability of daily precipitation events as a function of their duration and daily accumulation of the area-averaged precipitation over Afghanistan (box in Fig. 1). Two-dimensional probability curves are determined by tracking the number of events of varying duration and threshold, in increments of days and 0.25 mm, respectively. First, all dates in a month above a selected threshold are extracted, and the length of each string of consecutive dates exceeding that threshold is counted and binned. The number of events longer than each bin's duration are also summed and added to each duration's bin, to create cumulative distributions of event duration. Finally, each bin's event number is divided by the sum of all events in that month to attain the normalized probability of a precipitation event that is at least the value of that bin's duration and daily accumulation.

3. Results

3.1 Daily Precipitation Characteristics

Afghanistan's semi-arid climate receives most of its precipitation during the boreal cold season from November – April, during which time daily precipitation variance is generally comparable across IMERG, CHIRPS, JRA-55 and ERA5 datasets, while the gauge-based CPC dataset differs due to the limited number of stations in the region (Fig. 1). Daily statistics of area-averaged precipitation over Afghanistan (box in Fig. 1) also display good agreement among the various datasets considered, with the exception of the CPC estimate, and with better agreement between the standard deviation and 95th percentile values than the medians (Fig. 2), reflecting the non-Gaussian nature of precipitation (e.g., Papalexiou and Koutsoyiannis 2013). JRA55 displays the highest median and standard deviation, potentially related to the coarser horizontal

https://doi.org/10.5194/egusphere-2023-388
Preprint. Discussion started: 7 March 2023

resolution (0.56° compared to 0.25° for the other satellite-based estimates), and CPC's gauge-based estimates the lowest. A common element among all datasets is that precipitation median and standard deviation peak at different times within the wet season. The standard deviation increases from October to February and decreases thereafter, while median precipitation does not increase notably until January, and remains elevated through April. This means that while accumulation is greatest in February, March and April, the dynamics and circulation patterns associated with precipitation in February, when the standard deviation and extreme values peak, is likely different than the nature of precipitation in April, when median precipitation is still high, but variance has decreased. These differences in the circulation and characteristics of precipitation within the leading precipitation months from January to April is the focus of subsequent analysis in section 3.2.

Binning area-averaged total precipitation over Afghanistan (box in Fig. 1) by each day's accumulation value indicates that the greatest portion of precipitation occurs on the few days with daily accumulation > 4 mm (Fig. 3), which we will refer to as heavy precipitation days. While there are some differences between datasets concerning total precipitation amount, with CHIRPS showing lower accumulations and JRA55 the highest, the month-to-month evolution of the different accumulation groups is consistent among the three datasets for their common period, 1981-2020. In all datasets, each month is likely to expect about 1-6 days on average with heavy precipitation, a reflection of the intermittent and intense nature of precipitation (e.g., Pendergrass and Knutti 2018), with the intensity likely related in part to orographic enhancement of vertical motion. March displays the greatest accumulation, followed by February, with heavy precipitation days dominating accumulation in both months. In April, the number heavy precipitation days decreases, while the contributions from values < 4 mm are elevated compared to earlier in the season, accounting for the reduction in standard deviation and 95th percentile precipitation values observed in Figure 2, while the median is similar to February and March. Overall, April is one of the top months for total precipitation, with totals similar or higher to the amount that occurs in January, depending on the dataset. Few heavy precipitation events last longer than a couple of days, with the longest events occurring in March and February (Fig. S1), consistent with the greatest number of heavy precipitation events observed during these months (Fig. 3). No heavy precipitation events are observed to last longer than a week in all datasets, with one-day events accounting for the majority, reflecting the sporadic nature of precipitation in this area.

Considering the joint probability of precipitation duration and amplitude further confirms how precipitation events evolve from winter into spring, with more short, extreme events during the former and longer, weak events during the latter (Fig. 4; Fig. S2). The warm colors indicate the least likely but high accumulation precipitation events, while the highest probability contour in blue indicates more likely, lower accumulation events of less consequence. The constant liquid equivalent values shown in dashed black lines indicate where the accumulation of events with different duration and intensity is equal. In October, precipitation is generally scarce, with only short, low-amplitude events observed and probability values clustered around low accumulations in the bottom-left corner (Fig. 4a). In January and April, precipitation becomes more intense and more persistent, with increases in the likelihood of high accumulation events relative to October (Fig. 4b-c). Comparing events in January and April, which have comparable mean precipitation, there are clear differences in how precipitation occurs, which was suggested by the differences in total accumulation contributed from various daily accumulation

https://doi.org/10.5194/egusphere-2023-388
Preprint. Discussion started: 7 March 2023

values (Fig. 3). Specifically, January has a greater occurrence of short, high-amplitude events that exceed 12 mm accumulation (c.f., top-left quadrant of Fig. 4b vs c) while April has a greater likelihood of long, low-amplitude events that can produce similar accumulation totals (c.f., bottom-right quadrant of Fig. 4b vs c). The next section will show that, in addition to these differences in precipitation duration and amplitude, the circulation associated with heavy precipitation days differs between January and April as well.

3.2 Warm Conveyor Belts and Precipitation

While seasonal and monthly mean precipitation over CSWA has been related to enhanced moisture transport in past studies (Mariotti 2007; Hoell et al. 2015a), the transient features that evolve on *daily* timescales and are related to precipitation have not been extensively considered, particularly regarding their month-to-month differences. The seasonality of the WCB frequency indicates that ascent associated with extratropical cyclones peaks from February to April, consistent with the timing of peak precipitation (Figs. 5-6). This is consistent with the results of Pfahl et al. 2014 who found annual CSWA precipitation was heavily related to WCBs and shows that this correspondence is greatest in late winter and early spring. WCBs are largely absent over the region from September – November, increasing in frequency through March and thereafter decreasing to very rare occurrences by June. The region affected by WCBs is oriented in a southwest-northeast manner across the middle east and southwest Asia (Fig. 6), on the cyclonic shear side of the upper-level jet. A similar tilt to the geopotential height anomalies associated with monthly CSWA precipitation anomalies was noted by Hoell et al. 2015a. However, while the jet is strongest in January and February, WCB frequency peaks in March and remains strong in April as well, when the jet has weakened substantially. This suggests that the upper-level storm track, which peaks when the jet is strongest in January-February (Barlow et al. 2016), is not the only factor influencing the frequency of WCBs, and more generally precipitation-producing westerly disturbances, in this area. A local maximum in WCB frequency over Pakistan develops in March and persists through May, which is not observed in December-February, also reflecting how WCBs change during the progression from winter to spring. Given the WCB definition, requiring strong ascent within two days near a sea level pressure minimum, it is possible that cyclonic disturbances with different characteristics develop at various parts of the year, in the different mean states represented by the jet. This is explored next by comparing the circulation between days with heavy or negligible precipitation.

The composite difference between wet (> 4 mm) and dry (< 0.04 mm) days in each month confirms that, as the mean state evolves from the heart of winter into spring, the transient features associated with heavy precipitation change as well (Fig. 7). In January and February, a southwest-northeast oriented, low-level trough-ridge couplet are observed, with strong moisture transport and ascent located in-between the trough and ridge (Fig. 7a-b). This tilt combined with the cyclonic shear of the jet (Fig. 6) is conducive to barotropic energy extraction, which can support the amplification of baroclinic waves (Mak and Cai 1989), and thus could be a mechanism for development in this region. The positive tilt can also be reflective of anticyclonic wavebreaking and deep stratospheric intrusions, which have been linked to precipitation over the Middle East (de Vries et al. 2018) and could also be a factor for CSWA precipitation at this time of year. A similar height pattern is observed at 200 hPa, though with an additional cyclone located over southeast Asia. Enhanced WCB frequency is collocated with the strong IVT over Afghanistan (Fig. 7e-f). In March, only a single 700-hPa cyclonic anomaly is observed, while the 200-hPa

https://doi.org/10.5194/egusphere-2023-388
Preprint. Discussion started: 7 March 2023

circulation involves a different pattern than December and January, with the hint of an anticyclonic anomaly located over northeast Africa that strengthens in April (Fig. 7g,h). The positive tilt to the anomalies observed in JFM is not present in April either, overall indicating a shift in the circulation associated with precipitation as winter transitions to spring that was similarly noted in Hoell et al. 2015a. Conciding with the circulation changes, WCB frequencies also shift to peaking over Afghanistan in January and February to over Pakistan in March and April (Fig. 6). April is also characterized by locations of negative WCB frequencies to the west of the cyclonic anomaly, indicating a coincident suppression of precipitation in areas beyond Afghanistan associated with this pattern that is not present in other months. We note that March is in the middle of the winter-to-spring transition, which likely means that early in the month, precipitation occurs due to patterns that resemble January-February, while later in the month the pattern resembles that in April, meaning the overall March pattern is a blend with only a common element of a cyclone to the west. Future work could break down each month's heavy precipitation days into groups with similar patterns to better understand the flavors of precipitation that are observed within each month, which could be particularly illuminating during transition months such as March.

3.3 Modulation by El Niño and La Niña conditions

As previously mentioned, one of the most predictable signals altering precipitation over Afghanistan, and more broadly CSWA, is ENSO (Hoell et al 2020; Breeden et al. 2022). To confirm that differences are robust across multiple precipitation estimates, we first consider monthly difference in CSWA precipitation using ENSO events that occurred between 1981-2017 (Table S1). Over this period, EN conditions are most often associated with enhanced precipitation compared to LN conditions, particularly in March, when most significant increase in WCB frequency is also observed (Fig. 8). The precipitation differences between the two phases are consistent among the CHIRPS, ERA5 and JRA55 datasets, except for in April when CHIRPS indicates no significant change in precipitation, while ERA5, JRA55 and WCBs all display significant differences. In January, conversely, no change in WCB frequency or precipitation is observed in any of the three precipitation datasets, which may initially be perplexing but is consistent with the lack of significant tropical Pacific SSTs associated with monthly CSWA precipitation anomalies in January (Hoell et al. 2015a). However, the precipitation dataset used by Hoell et al. 2015a was a reanalysis-based estimate that is adjusted using a blend of observational datasets, including satellite information, suggesting that the similarity between our and their results may be due to similar characteristics in the precipitation dataset, and may not serve as a fully independent verification. Nonetheless, the generally observed increased precipitation during EN conditions is consistent with past studies considering seasonal means (Mariotti et al. 2007; Hoell et al. 2012; Barlow et al. 2016; Hoell et al. 2018a). Higher mean precipitation during EN months is related to the increased occurrence of heavy precipitation days (Fig. 9), which increases from an average of 4.1 days in LN March to 5.9 days in EN March, and from 2.5 to 4.3 days in April LN and EN for ERA5 precipitation, respectively. As such, only a few days of heavy precipitation are strongly influencing monthly-mean and seasonal-mean shifts in hydroclimate over the region, consistent with past precipitation studies highlighting this disproportionate influence (Pendergrass and Knutti 2018). Furthermore, while there are two fewer EN March months than LN March months (9 versus 11), more precipitation accumulated during the former (Fig. 9a-b),

https://doi.org/10.5194/egusphere-2023-388
Preprint. Discussion started: 7 March 2023

underscoring the disproportionate effect that sporadic, heavy precipitation during El Niño conditions has on CSWA hydroclimate.

To better understand the month-to-month variations in precipitation during EN and LN conditions, we consider the composite IVT and WCBs in January, when precipitation and WCBs display no change between EN/LN conditions, and in March, when both display their strongest differences. In January, WCBs are overall rare in the region (Fig. 6; Fig. 10a,b), with only small increases in WCB frequency observed during EN months, to the north of Afghanistan that are collocated with a positive precipitable water anomaly and enhanced northeastward IVT (Fig. 10c). Conversely, in March, WCBs are more frequent over a large area including Afghanistan, Pakistan, and northwestern China during EN compared to LN months (Fig. 10d-f). Positive differences in precipitable water between EN and LN months are observed locally and, to a larger extent, over the Arabian Peninsula, collocated with stronger southwesterly/westerly flow transporting moisture from lower latitudes to CSWA. The pattern of enhanced IVT is similar to the regression of IVT onto Niño3.4 in DJF (Mariotti et al. 2007). As such, during EN conditions, both vertical motion from synoptic systems *and* moisture availability from lower latitudes are strengthened, increasing precipitation, except in January when neither change. On heavy precipitation days during March EN months, a stronger cyclonic anomaly and higher WCB frequencies are observed than on March LN days (Fig. S3), consistent with enhanced ascent and precipitation during the former. WCBs and IVT also increase notably in February and April, in a similar manner to March, though WCB changes in in February are less uniform and mainly located to the south over Pakistan (Fig. S4). Overall, the exact timing of the biggest ENSO influence on the circulation and precipitation appears to be in March and April, rather than earlier in the winter such as January, when the climatological paucity of WCBs seems to limit the influence on precipitation. However, revisiting these month-to-month precipitation differences with a larger sample size using climate model ensembles, for instance, would be advantageous.

4 Discussion and Conclusions

This study compared the evolution of daily CSWA precipitation as estimated by several modern precipitation datasets, with a focus on Afghanistan, to complement the consideration given to monthly and seasonal mean precipitation characteristics, which have been the primary focus of many past studies. Precipitation estimates that incorporate satellite information display generally good agreement during the wet season, while the gauge-based CPC dataset suggests a lower estimate that differs substantially, given the sparse network of gauges in the area. Precipitation mainly occurs during sporadic, high-amplitude events during the cold season, with the patterns associated with precipitation evolving from a dipole-type pattern, indicated by a couplet of streamfunction anomalies, in January and February into a single cyclonic monopole pattern by April. The dipole pattern observed in January and February is similar to the 'central Asian weather type' identified by Gerlitz et al. 2018, who used k-means clustering over a large domain over central Asia to isolate different patterns of atmospheric variability during boreal winter (thus excluding April). The 'central Asia' pattern was the least frequent of the eight identified, consistent with the infrequency of precipitation in this region relative to others; this pattern also displayed the strongest precipitation anomalies over Afghanistan of all considered, consistent with the present analysis. Peak WCB frequency from February - April occurs later than the peak strength of the upper-level jet and storm track in DJF, suggesting

https://doi.org/10.5194/egusphere-2023-388
Preprint. Discussion started: 7 March 2023

that, in this region, upper-level dynamical forcing is not the only factor modulating the frequency of WCBs (Fig. 6). As such, understanding the lifecycle of cyclones and exploring changes in relevant factors, such as static stability, in this area could be a future avenue of research.

The sporadic nature of precipitation has been highlighted from a global perspective by Pendergrass and Knutti (2018), who also emphasized the disproportionate impact that only a handful of precipitation events has on the seasonal and annual mean distribution. This uneven impact is reflected here for CSWA and highlights the region's susceptibility to drought, such as the one during the 1999-2001 La Niña (Barlow et al. 2002), when only 31 days with an accumulation exceeding 4 mm were observed in three years. This is roughly half of the long-term average of about 20 days per year with the same accumulation (Fig. 3), meaning that a leading impact of ENSO is to modulate the number of heavy precipitation days observed (Fig. 9). WCBs evolve on a similar temporal scale as precipitation by definition, and through their link to extratropical cyclones (Madonna et al. 2014), are intuitively related to strong precipitation events. Showing that their frequency over CSWA is modulated by ENSO phase further clarifies the link between the low-frequency circulation changes that ENSO produces, and the transient, short-lived nature of precipitation in this region. The lack of CSWA precipitation sensitivity to tropical SSTs in January that was found by Hoell et al. 2015a is consistent with the similarity in WCBs between EN and LN conditions observed in January in this study. Why January in particular lacks such a link to tropical SSTs and ENSO, which is apparent in the other cold-season months, remains to be determined and merits further investigation.

Finally, we note that the choice of the Niño3.4 index to capture ENSO variability is motivated by the wide use and public availability of this index, and the fact that central Pacific ENSO events in particular appear to have an effect on southwest Asian climate (Hoell et al. 2018a). It is true, however, that CSWA may be sensitive to certain characteristics of each ENSO event, such as the strength of the associated east-west SST gradient (Hoell et al. 2013), which is not necessarily captured by Niño3.4. Furthermore, there are alternative methods than indices of SST anomalies that have also proven useful in capturing the full scope of ENSO's influence (Penland and Sardeshmukh 1995) and its impact on regional climate (Albers et al. 2021; Albers et al. 2022; Breeden et al. 2022). Future work could make use of these dynamically-based techniques and revisit the question of ENSO's influence on central southwest Asian precipitation. Experiments generating larger samples of ENSO events in each month, as conducted in Albers et al. 2022, would also be useful to revisit the month-to-month variations in ENSO's influence found in this study.

Data Availability

The JRA-55 Reanalysis data used in this study are freely available at https://doi.org/10.5065/D6HH6H41 (Japan Meteorological Agency, 2013), and CHIRPS precipitation is freely available at https://data.chc.ucsb.edu/products/CHIRPS-2.0/global_daily/netcdf/p25/ (Climate Hazards Center, 2021). CPC Global Unified Gauge-Based Analysis of Daily Precipitation data was provided by the NOAA PSL, Boulder, Colorado, USA, from their website at https://psl.noaa.gov. ERA5 Reanalysis data is freely available online: https://cds.climate.copernicus.eu/cdsapp#!/dataset/reanalysis-era5-single-levels?tab=overview. IMERG data is freely available online: https://gpm.nasa.gov/data/directory.

https://doi.org/10.5194/egusphere-2023-388
Preprint. Discussion started: 7 March 2023

Author Contributions: MLB acquired data, wrote code for calculations, produced all figures, and wrote the manuscript. AH and JRA offered guidance on relevant topics and datasets and provided input on figures and edits to the manuscript. KS provided input on figures and edits to the manuscript.

Competing interests: The contact author has declared that none of the authors has any competing interests.

Acknowledgements: The authors gratefully acknowledge Dr. Michael Sprenger for generating the WCB dataset and Dr. Benjamin Moore for locally providing 6-hourly WCB dataset, and financial support from the Famine Early Warning Systems Network and United States Agency for International Development.

References

Albers, J. R. and Newman M.: Subseasonal predictability of the North Atlantic Oscillation, Environmental Research Letters, 16 (4), 044024, 2021.

Albers, J. R., Newman, M., Hoell, A., Breeden, M. L., Wang, Y., and Lou, J.: The February 2021 Cold Air Outbreak in the United States: a Subseasonal Forecast of Opportunity, *Bulletin of the American Meteorological Society*, published online ahead of print, DOI: https://doi.org/10.1175/BAMS-D-21-0266.1, 2022.

Barlow, M., Cullen, H., and Lyon, B.: Drought in central and southwest Asia: La Niña, the warm pool, and Indian Ocean precipitation, J. Climate, 15, 697–700, https://doi.org/10.1175/1520- 0442(2002)015<0697:DICASA>2.0.CO;2, 2002.

Barlow, M., and M. K. Tippett: Variability and predictability of central Asia river flows: Antecedent winter precipitation and large-scale teleconnections, J. Hydrometeor., 9, 1334–1349, doi:10.1175/2008JHM976.1, 2008.

Barlow, M., Zaitchik, B., Paz, S., Black, E., Evans, J., and Hoell, A.: A Review of Drought in the Middle East and Southwest Asia, J. Climate, 29, 8547–8574, 2016.

Breeden, M. L., Albers, J. R., A. Hoell: Subseasonal precipitation forecasts of opportunity over southwest Asia, *Wea. Clim. Dynam.*, *3*, 1183–1197, https://doi.org/10.5194/wcd-3-1183-2022, 2022.

Cannon, F., Carvalho, L. M. V., Jones, C., Hoell, A., Norris, J., Kiladis, G. N., and Tahir, A. A.: The influence of tropical forcing on extreme winter precipitation in the western Himalaya, Clim. Dy- nam., 48, 1213–1232, https://doi.org/10.1007/s00382-016-3137- 0, 2017.

https://doi.org/10.5194/egusphere-2023-388
Preprint. Discussion started: 7 March 2023

Chen, M., W. Shi, P. Xie, V. B. S. Silva, V. E. Kousky, R. W. Higgins, and Janowiak, J. E.: Assessing objective techniques for gauge-based analyses of global daily precipitation. J. Geophys. Res., 113, D04110, 2008.

Climate Hazards Center (CHC) University of California at Santa Barbara (UCSB), '# Afghanistan Stations in monthly CHIRPS-v2.0, https://data.chc.ucsb.edu/products/CHIRPS-2.0/diagnostics/stations-perMonth-byCountry/pngs/Afghanistan.066.station.count.CHIRPS-v2.0.png, last accessed February 27, 2023.

de Vries, A. J., Ouwersloot, H. G., Feldstein, S. B., Riemer, M., El Kenawy, A. M., McCabe, M. F., & Lelieveld, J.: Identification of tropical-extratropical interactions and extreme precipitation events in the Middle East based on potential vorticity and moisture transport. Journal of Geophysical Research: Atmospheres, 123, 861–881, 2018.

FAO, IFAD, UNICEF, WFP and WHO: The State of Food Security and Nutrition in the World 2022. Repurposing food and agricultural policies to make healthy diets more affordable. Data are available on FAOSTAT (https://www.fao.org/faostat/en/#data/FS), 2022.

FEWS NET: Afghanistan Food Security Outlook February to September 2018: Low snow accumulation and dry soil conditions likely to impact 2018 staple production, https://fews.net/sites/default/files/documents/reports/AFGHANISTANFoodSecurityOutlook_Feb_Sept2018.pdf (last access: 28 June 2022), 2018.

Funk, C., Peterson, P., Landsfeld, M. Pedreros, D., Verdin, J., Shukla, S., Husak, G., Rowland, J., Harrison, L., Hoell, A., and J. Michaelsen: The climate hazards infrared precipitation with stations – a new environmental record for monitoring extremes, Sci Data, 2, 150066, https://doi.org/10.1038/sdata.2015.66, 2015.

Funk, C., Shukla, S., Thiaw, W. M., Rowland, J., Hoell, A., McNally, A., Husak, G., Novella, N., Budde, M., Peters-Lidard, C., Adoum, A., Galu, G., Korecha, D., Magadzire, T., Rodriguez, M., Robjhon, M., Bekele, E., Arsenault, K., Peterson, P., Harrison, L., Fuhrman, S., Davenport, F., Landsfeld, M., Pedreros, D., Jacob, J. P., Reynolds, C., Becker-Reshef, I., and Verdin, J.: Recognizing the Famine Early Warning Systems Network: Over 30 Years of Drought Early Warning Science Advances and Partnerships Promoting Global Food Security, *Bulletin of the American Meteorological Society*, *100*(6), 1011-1027, 2019.

Gerlitz, L., Steirou, E., Schneider, C., Moron, V., Vorogushyn, S., and Merz, B.: Variability of the Cold Season Climate in Central Asia. Part I: Weather Types and Their Tropical and Extratropical Drivers, *Journal of Climate*, *31*(18), 7185-7207, 2018.

https://doi.org/10.5194/egusphere-2023-388
Preprint. Discussion started: 7 March 2023

Gerlitz, L. Vorogushyn S. and Gafurov, A.: Climate informed seasonal forecast of water availability in Central Asia: State-of-the-art and decision making context, *Water Security*, 10 (2020) 100061, 2020.

Green, J. S. A., F. H. Ludlam, and McIlveen, J. F. R.: Isentropic relative-flow analysis and the parcel theory. Quart. J. Roy. Meteor. Soc., 92, 210–219, 1966.

Hagen, E., Teufert, J.F.: Flooding in Afghanistan: A Crisis. In: Jones, J.A.A., Vardanian, T.G., Hakopian, C. (eds) Threats to Global Water Security. NATO Science for Peace and Security Series C: Environmental Security. Springer, Dordrecht. https://doi-org.colorado.idm.oclc.org/10.1007/978-90-481-2344-5_19, 2009.

Hersbach, H., and Coauthors: The ERA5 global reanalysis. Quart. J. Roy. Meteor. Soc., 146, 1999–2049, https://doi.org/10.1002/qj.3803, 2020

Hoell, A., Barlow, M., and Saini, R.: The leading pattern of intraseasonal and interannual Indian Ocean precipitation variability and its relationship with Asian circulation during the boreal cold sea- son, J. Climate, 25, 7509–7526, https://doi.org/10.1175/JCLI-D- 11-00572.1, 2012.

Hoell, A., C. Funk, and M. Barlow: The regional forcing of Northern hemisphere drought during recent warm tropical west Pacific Ocean La Niña events. Climate Dyn., 42, 3289– 3311, doi:10.1007/s00382-013-1799-4, 2013.

Hoell, A., C. Funk, and Barlow M.: The regional forcing of Northern Hemisphere drought during recent warm tropical west Pacific Ocean La Niña events. Climate Dyn., 42, 3289–3311, doi:10.1007/s00382-013-1799-4, 2014a.

Hoell, A., C. Funk, and Barlow M.: La Niña diversity and northwest Indian Ocean Rim teleconnections. Climate Dyn., 43, 2707–2724, doi:10.1007/s00382-014-2083-y, 2014b.

Hoell, A., S. Shukla, M. Barlow, F. Cannon, C. Kelley, and C. Funk: The forcing of monthly precipitation variability over southwest Asia during the boreal cold season. J. Climate, 28, 7038–7056, doi:10.1175/JCLI-D-14-00757.1, 2015a.

Hoell, A., Funk, C., and Barlow, M.: The Forcing of Southwestern Asia Teleconnections by Low-Frequency Sea Surface Temperature Variability during Boreal Winter, *Journal of Climate*, *28*(4), 1511-1526, 2015b.

https://doi.org/10.5194/egusphere-2023-388
Preprint. Discussion started: 7 March 2023

Hoell, A., M. Barlow, F. Cannon, and T. Xu, 2017a: Oceanic origins of historical southwest Asia precipitation during the boreal cold season. J. Climate, 30, 2885–2903, https://doi.org/10.1175/ JCLI-D-16-0519.1.

Hoell, A., Barlow, M., Xu, T., and Zhang, T.: Cold Season South- west Asia Precipitation Sensitivity to El Niño–Southern Oscilla- tion Events, J. Climate, 31, 4463–4482, 2018a.

Hoell, A., Cannon, F., and Barlow, M.: Middle East and South- west Asia Daily Precipitation Characteristics Associated with the Madden–Julian Oscillation during Boreal Winter, J. Climate, 31, 8843–8860, 2018b.

Hoell, A., Eischeid, J., Barlow, M., and McNally, A.: Character- istics, precursors, and potential predictability of Amu Darya Drought in an Earth system model large ensemble, Clim. Dynam., 55, 2185–2206, https://doi.org/10.1007/s00382-020- 05381-5, 2020.

Huffman, G. J., Bolvin, D. T., Braithwaite, D., Hsu, K.-L., Joyce, R. J., Kidd, C., Nelkin, E. J., Sorooshian, S., Stocker, E. F., Tan, J., Wolff, D. B., and Xie, P.: Integrated Multi-satellite Re- trievals for the Global Precipitation Measurement (GPM) Mission (IMERG), in: Satellite Precipitation Measurement: Volume 1, edited by: Levizzani, V., Kidd, C., Kirschbaum, D. B., Kummerow, C. D., Nakamura, K., and Turk, F. J., Springer Inter- national Publishing, Cham, 343–353, ISBN 978-3-030-24568-9, https://doi.org/10.1007/978-3-030-24568-9_19, 2020.

Kobayashi, S., Ota, Y., Harada, Y., Ebita, A., Moriya, M., Onoda, H., Onogi, Kamahori, H., Kobayashi, C., Hirokazu, E., Miyaoka, K., and Takahashi, K.: The JRA-55 reanalysis: General specifi- cations and basic characteristics. J. Meteorol. Soc. Jpn. Ser. II, 93, 5–48, https://doi.org/10.2151/jmsj.2015-001, 2015.

Lang, T.J., Barros A. P.: Winter storms in the central Himalayas. J Meteorol Soc Jpn 82:829–844, 2004.

Lotsch, A., M. A. Friedl, B. T. Anderson, and C. J. Tucker: Response of terrestrial ecosystems to recent Northern Hemispheric drought. Geophys. Res. Lett., 32, L06705, doi:10.1029/2004GL022043, 2005.

Mariotti A.: How ENSO impacts precipitation in southwest central Asia. Geophys Res. Lett., 34:1–5, 2007.

Madonna, E., H. Wernli, H. Joos, and O. Martius: Warm conveyor belts in the ERA-Interim dataset (1979–2010). Part I: Climatology and potential vorticity evolution. J. Climate, 27, 3–26. doi: http://dx.doi.org/10.1175/JCLI-D-12-00720.1, 2014.

Mak, M. and Cai, M.: Local barotropic instability. Journal of the Atmospheric Sciences, 46, 3289–3311, 1989.

https://doi.org/10.5194/egusphere-2023-388
Preprint. Discussion started: 7 March 2023

McNally, A., Jacob, J., Arsenault, K., Slinski, K., Sarmiento, D. P., Hoell A., Pervez, S., Rowland J., Budde, M, Kumar S., Peters-Lidard, C., and Verdin, J. P.: A Central Asia hydrologic monitoring dataset for food and water security applications in Afghanistan. Ear. Syst. Sci. Data, 14, 3115–3135, https://doi.org/10.5194/essd-14-3115-2022, 2022.

Nazemosadat, M. J., and A. R. Ghasemi: Quantifying the ENSO-related shifts in the intensity and probability of drought and wet periods in Iran. J. Climate, 17, 4005–4018, https://doi.org/ 10.1175/1520-0442(2004)017,4005:QTESIT.2.0.CO;2, 2004.

Papalexiou, S. M., and D. Koutsoyiannis: Battle of extreme value distributions: A global survey on extreme daily rainfall, Water Resour. Res., 49, doi:10.1029/2012WR012557, 2013.

Pendergrass, A. G., and Knutti, R.: The uneven nature of daily precipitation and its change. Geophysical Research Letters, 45, 11,980–11,988. https://doi. org/10.1029/2018GL080298, 2018.

Pfahl, S., Madonna, E., Boettcher, M., Joos, H., and Wernli, H.: Warm Conveyor Belts in the ERA-Interim Dataset (1979–2010). Part II: Moisture Origin and Relevance for Precipitation, *Journal of Climate*, *27*(1), 27-40, 2014.

Qutbudin, I.; Shiru, M.S.; Sharafati, A.; Ahmed, K.; Al-Ansari, N.; Yaseen, Z.M.; Shahid, S.; Wang, X.: Seasonal Drought Pattern Changes Due to Climate Variability: Case Study in Afghanistan. *Water* , *11*, 1096. https://doi.org/10.3390/w11051096, 2019.

Sprenger, M., Fragkoulidis, G., Binder, H., Croci-Maspoli, M., Graf, P., Grams, C. M., Knippertz, P., Madonna, E., Schemm, S., Škerlak, B., & Wernli, H.: Global Climatologies of Eulerian and Lagrangian Flow Features based on ERA-Interim, *Bulletin of the American Meteorological Society*, *98*(8), 1739-1748, 2017.

Sun, Q., Miao, C., Duan, Q., Ashouri, H., Sorooshian, S., & Hsu, K.-L.: A review of global precipitation data sets: Data sources, estimation, and inter- comparisons. Reviews of Geophysics, 56, 79–107. https://doi.org/10.1002/ 2017RG000574, 2018.

Thenkabail, P. S., M. S. D. N. Gamage, and V. U. Smakhtin: The use of remote-sensing data for drought assessment and monitoring in Southwest Asia. International Water Management Institute (Colombo, Sri Lanka) Research Rep. 85, 25 pp, 2004.

Trenberth, K. E.: The definition of El Niño, B. Am. Meteorol. Soc., 78, 2771–2778, https://doi.org/10.1175/1520-0477(1997)078<2771:TDOENO>2.0.CO;2, 1997.

https://doi.org/10.5194/egusphere-2023-388
Preprint. Discussion started: 7 March 2023

Trenberth, K. E., Zhang, Y. and M. Gehne: Intermittency in Precipitation: Duration, Frequency, Intensity, and Amounts Using Hourly Data. J. Hydrometeor., Volume 18, pp. 1393-1412. DOI: https://doi.org/10.1175/JHM-D-16-0263.1, 2017.

Wernli, H., and Davies, H. C.: A Lagrangian-based analysis of ex- tratropical cyclones. I: The method and some applications. Quart. J. Roy. Meteor. Soc., 123, 467–489, 1997.

Dataset	Period Considered	Horizontal Resolution	Temporal Resolution
CHIRPS	1981-2020	0.25x0.25°	Daily
IMERG	2001-2019	0.25x0.25°	Daily
JRA55	1981-2020	0.56x0.56°	Daily
ERA5	1981-2020	0.25x0.25°	Daily
CPC	1981-2020	0.5x0.5°	Daily

Table 1: Summary of precipitation data used in this study: Japanese Meteorological Agency 55-year Reanalysis (JRA-55; Kobayashi et al. 2015); Climate Hazards InfraRed Precipitation with Stations (CHIRPS; Funk et al. 2015); European Centre for Medium-Range Forecasting (ECMWF) Reanalysis v5 (ERA5; Hersbach et al. 2020); Integrated Multi-satellitE Retrievals for GPM version 06 (IMERG; Huffman et al. 2019); and the NOAA Climate Prediction Center (CPC) United Gauge Product (Chen et al. 2008). Note that the 'temporal resolution' and 'data period used' columns indicate the time periods used in this study, and that each product may also be available at higher temporal resolution (ie, IMERG) or spatial resolution (ie, CHIRPS).

https://doi.org/10.5194/egusphere-2023-388
Preprint. Discussion started: 7 March 2023

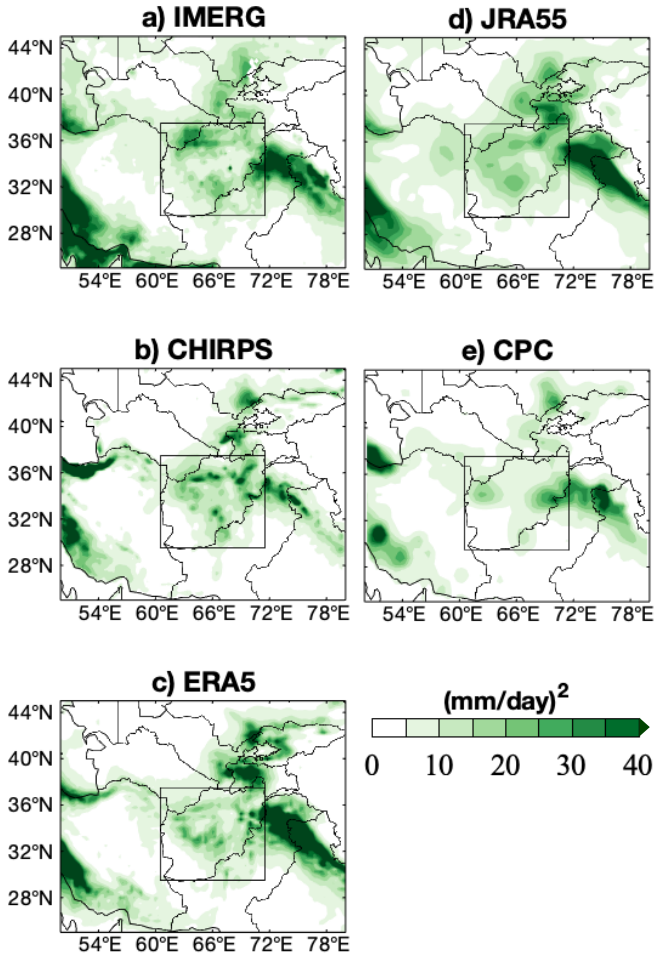

Figure 1: November - April 2001-2019 precipitation variance for a) IMERG b) CHIRPS c) ERA5, d) JRA55 and e) CPC datasets. The black square outlines the domain where daily precipitation is averaged (29.5-37.5°N, 60.5-71.5°E). See Table 1 for details about each product.

https://doi.org/10.5194/egusphere-2023-388
Preprint. Discussion started: 7 March 2023

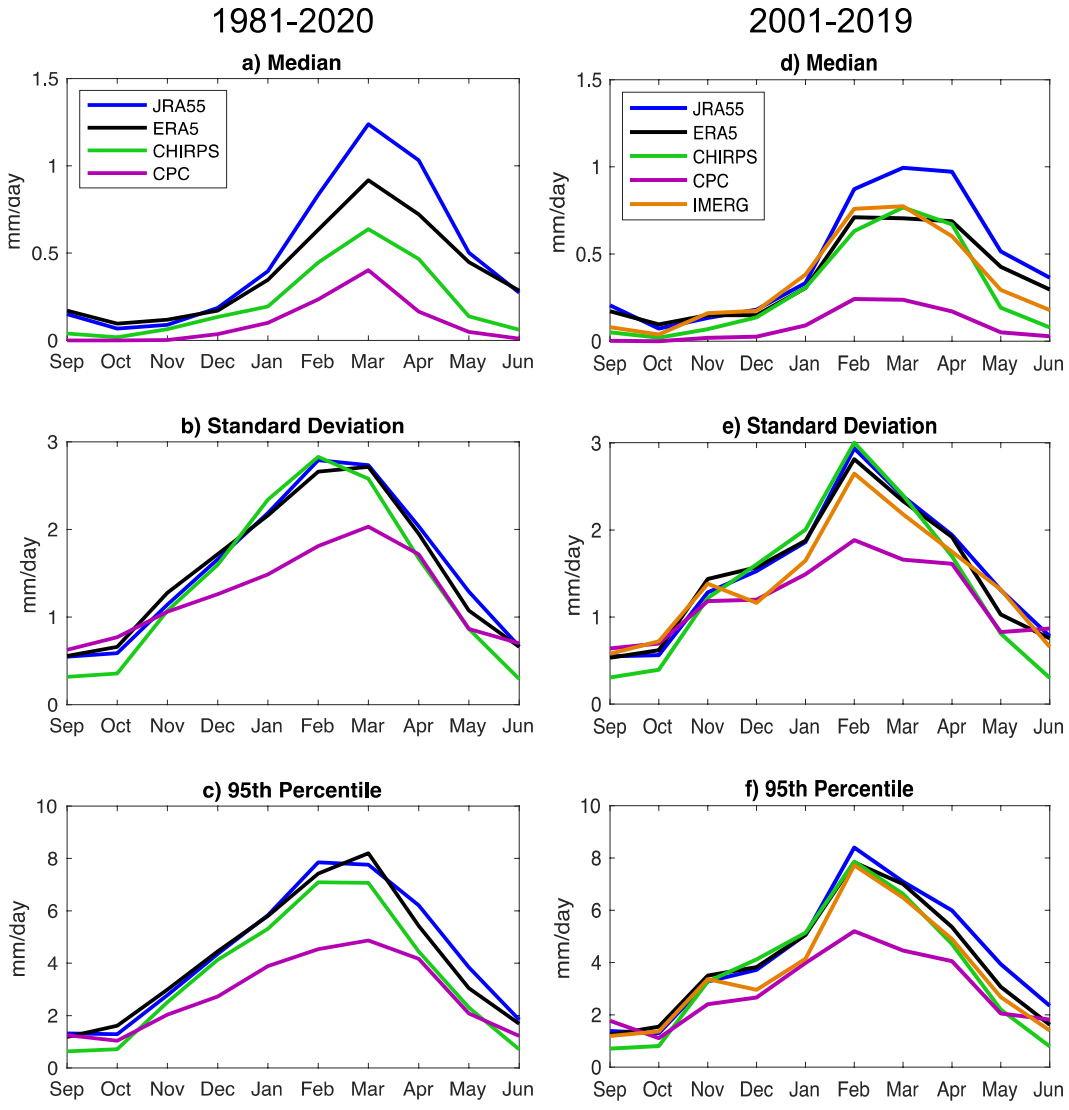

Figure 2: Monthly evolution of daily mean precipitation median, standard deviation, and 95th percentile for CHIRPS, ERA5, IMERG and JRA55 datasets, for their common periods a) – c) 1981-2020 and d) – f) 2001-2019 averaged over Afghanistan (box in Figure 1). IMERG is also shown for the 2001-2019 periods.

https://doi.org/10.5194/egusphere-2023-388
Preprint. Discussion started: 7 March 2023

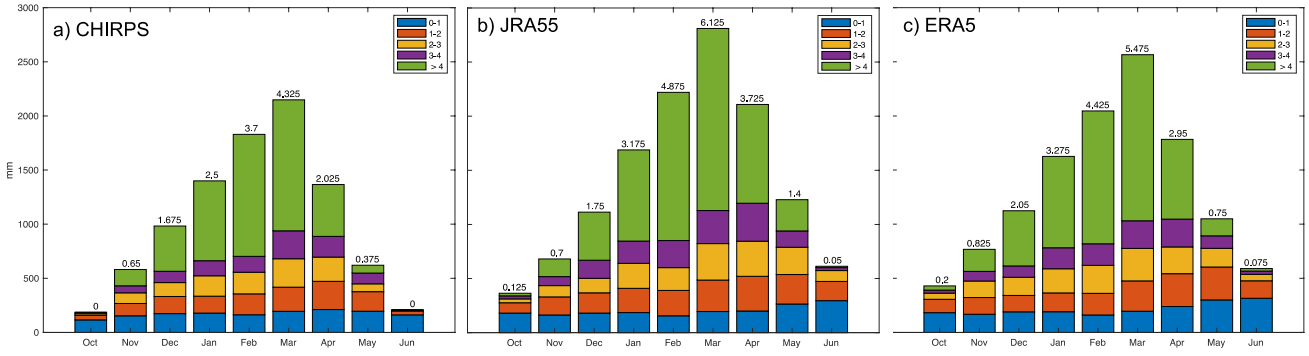

Figure 3: Cumulative a) CHIRPS, b) JRA55 and c) ERA5 precipitation, binned by daily rate, for the years 1981-2020. The numbers at the top of each column indicate the average number of days per year with accumulation > 4 mm.

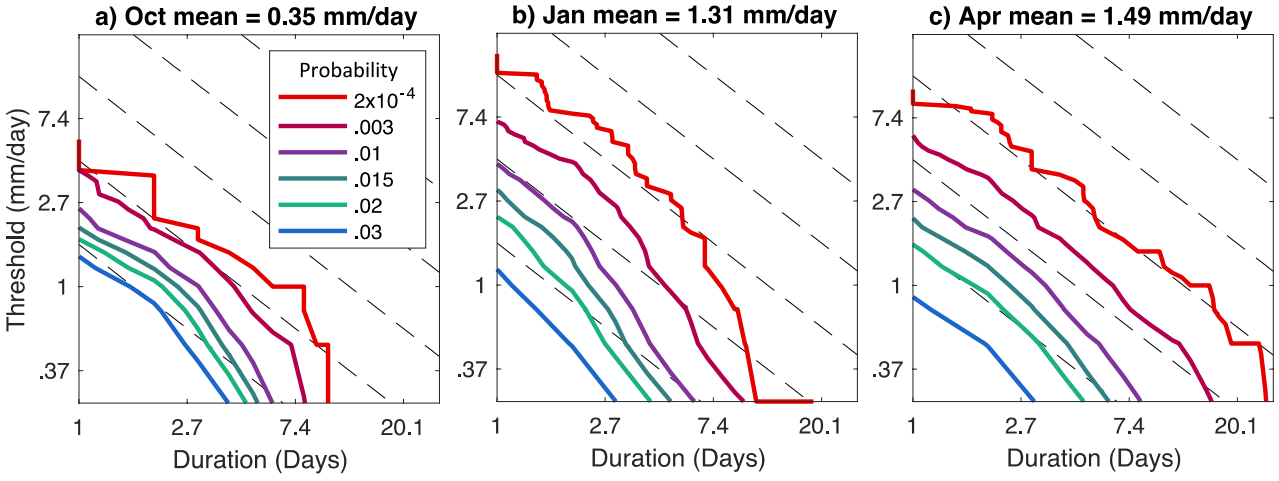

Figure 4: The thick solid contours show the joint probability of daily ERA5 precipitation intensity and duration for a) October b) January and c) April, 1981-2020. The black dashed contours indicate lines of constant liquid equivalent for the values: 1.65, 4.48, 12.2, 33.1, and 90 mm (starting in the lower-left corner to upper-right).

https://doi.org/10.5194/egusphere-2023-388
Preprint. Discussion started: 7 March 2023

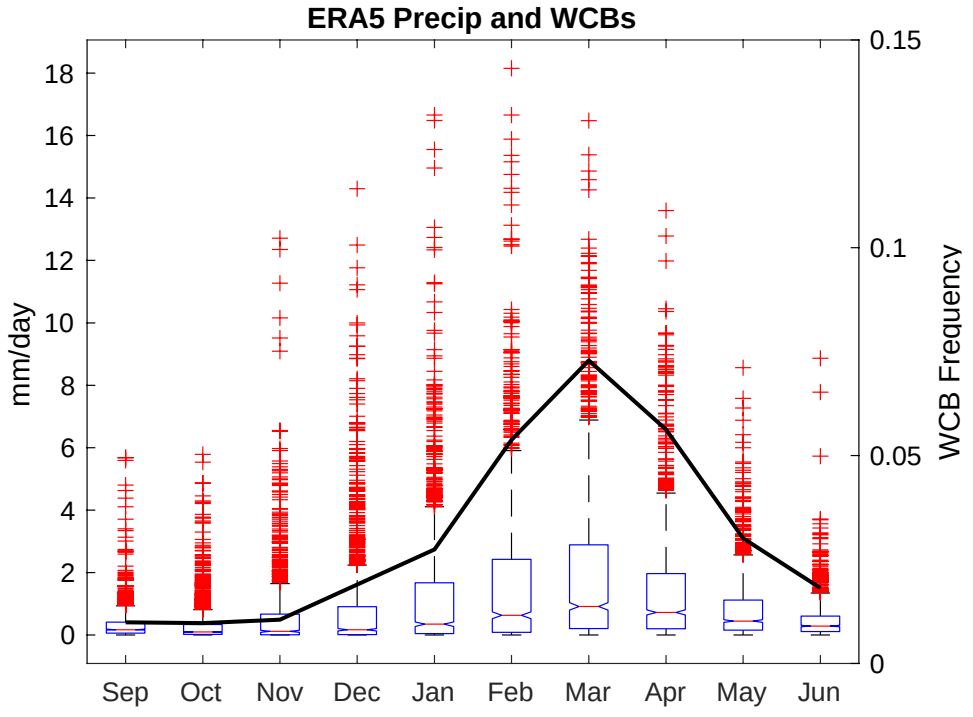

530 **Figure 5: Statistical distribution of ERA5 precipitation for September – June 1981-2020 (blue boxes and red '+' signs), and mean WCB frequency 1979-2017 (thick black line; units events/6-hourly time step), both fields averaged over Afghanistan (box in Fig. 1). For precipitation, the interquartile range for each month is shown in the blue boxes, with the median indicated by the red line. Outliers are shown in the red '+' signs.**

535

https://doi.org/10.5194/egusphere-2023-388
Preprint. Discussion started: 7 March 2023

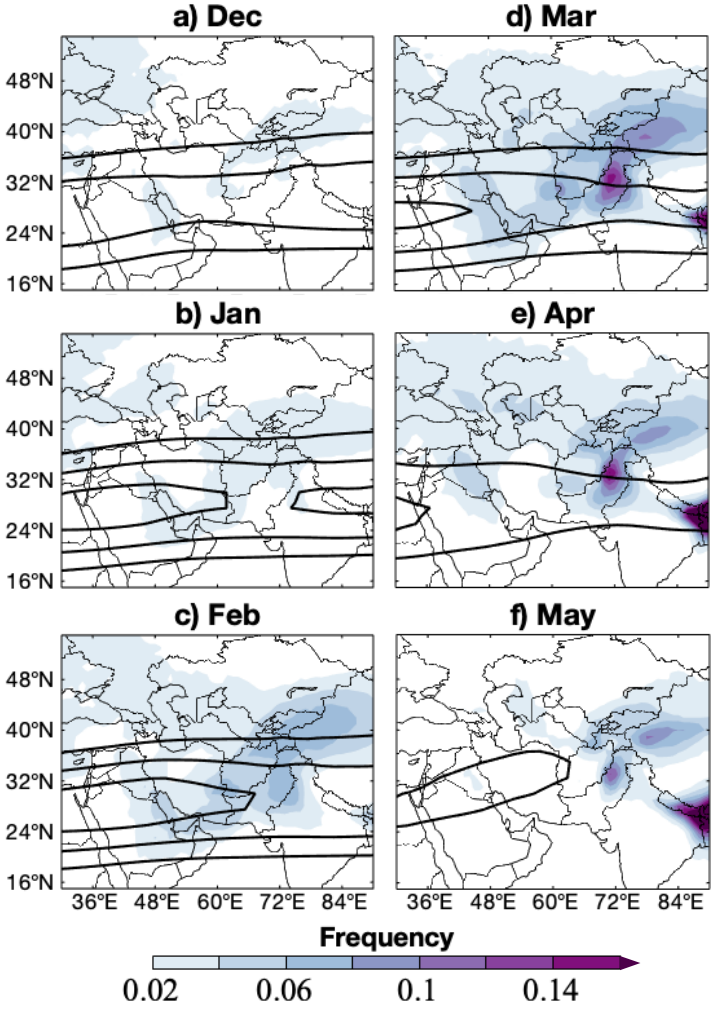

Figure 6: The color shading shows monthly mean WCB frequency in units of events per 6-hourly time step. The black contours show monthly mean 200-hPa zonal wind, contoured at 30 m s^{-1} every 10 m s^{-1}.

https://doi.org/10.5194/egusphere-2023-388
Preprint. Discussion started: 7 March 2023

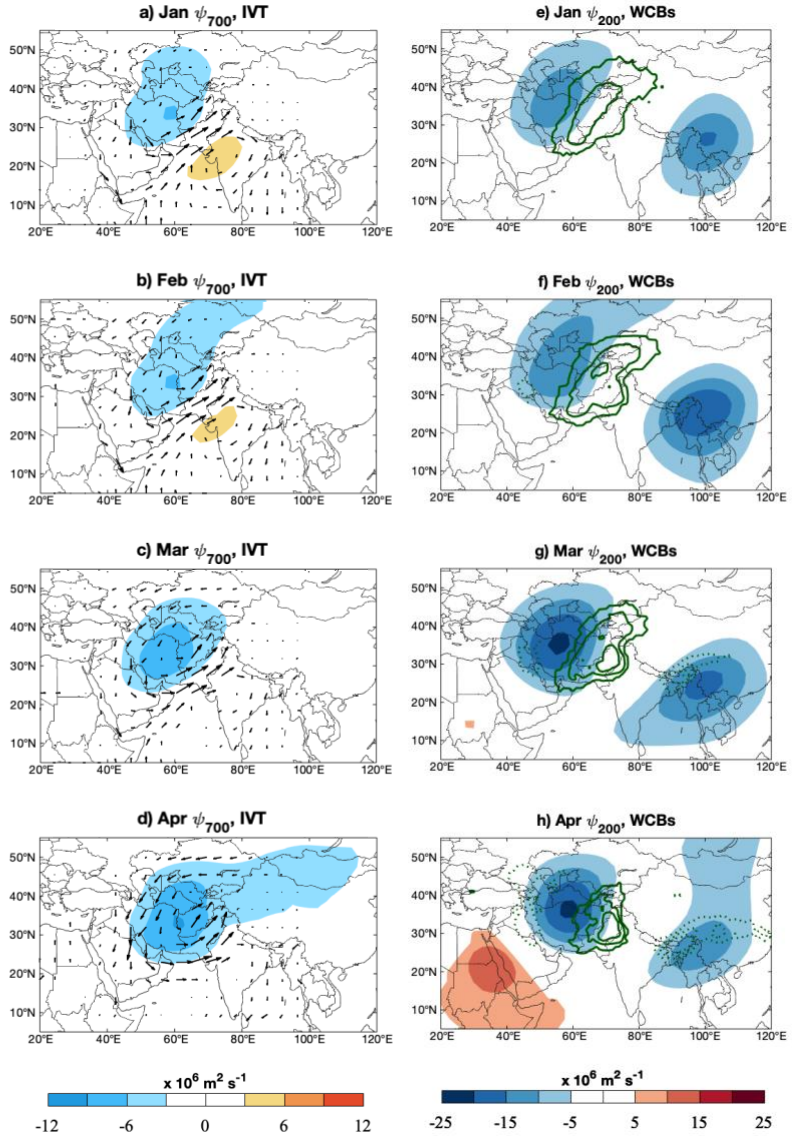

Figure 7: Composite difference between 'wet' days – meaning > 4 mm accumulation days - subtracted from 'dry' days, when precipitation < 0.04 mm. For the months January – April, panels a) – d) show 700-hPa streamfunction in the color shading and IVT in the vectors, and panels e) – h) show 200-hPa streamfunction in the color shading and WCB frequency in the green contours, contoured at .1 starting at +/- 0.05, positive frequencies (solid) and negative frequencies (dotted). WCB units are events/6-hourly time step. Only differences that are statistically significantly different from random chance at the 95th confidence level, determined using bootstrapping with replacement, are shown. The number of dry days in each composite is: 278 (Jan), 198 (Feb), 121 (Mar), 105 (Apr), and the number of wet days is: 122 (Jan), 164 (Feb), 203 (Mar), 106 (Apr).

https://doi.org/10.5194/egusphere-2023-388
Preprint. Discussion started: 7 March 2023

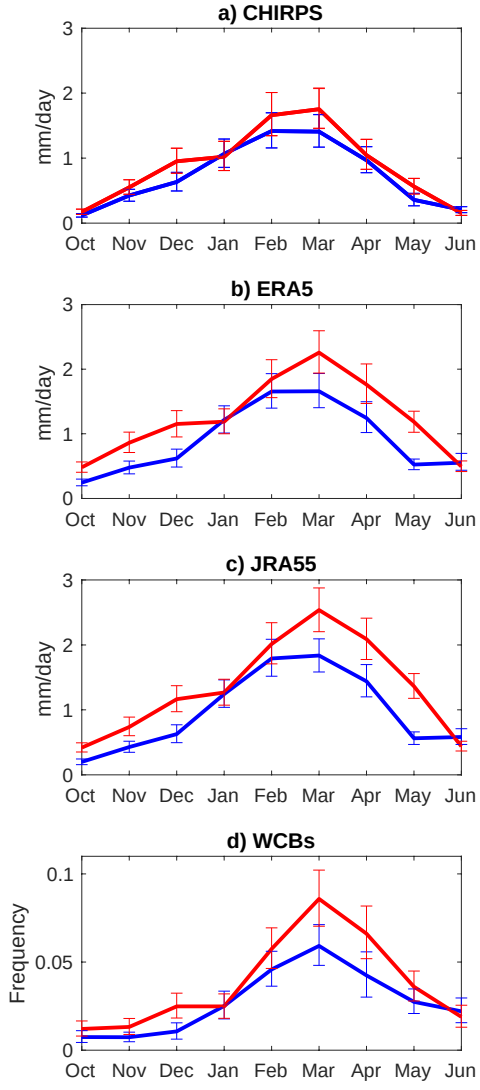

555 **Figure 8: Mean precipitation during El Niño (EN; red) and La Niña (LN; blue) months, determined using the ONI index, in a) CHIRPS, b) ERA5, c) JRA55 precipitation. Panel d) shows the mean WCB frequency (units events/6-hourly time step) during EN (red) and LN (blue) months. The error bars denote confidence at the 95% confidence interval, determined using bootstrapping with replacement.**

560

https://doi.org/10.5194/egusphere-2023-388
Preprint. Discussion started: 7 March 2023

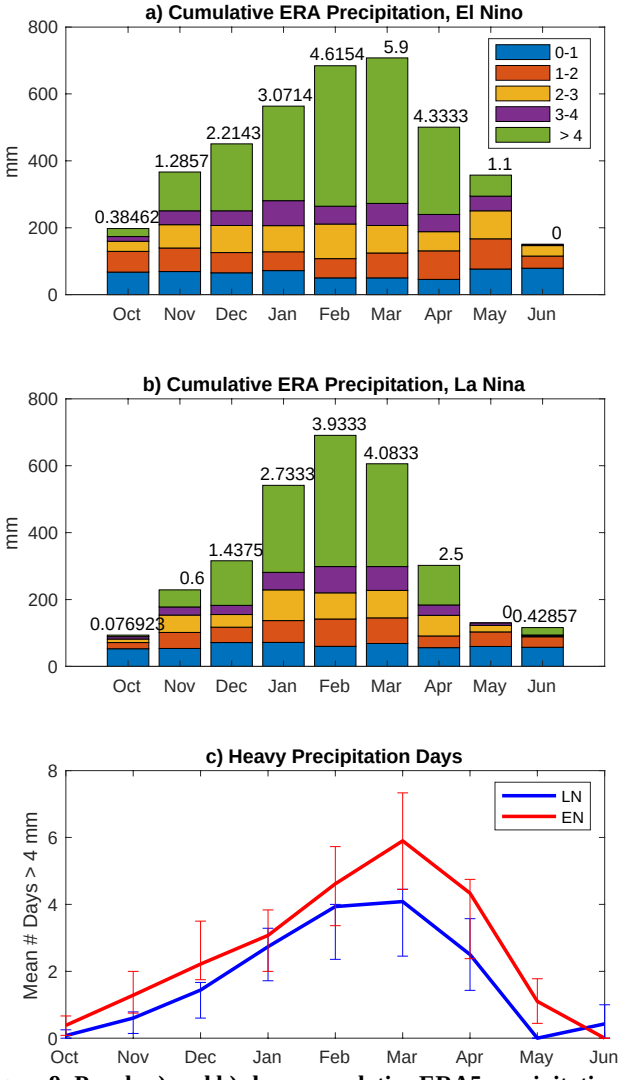

Figure 9: Panels a) and b) show cumulative ERA5 precipitation binned by daily rate during El Nino and La Nina months (Table S1) that occurred from 1981-2017, respectively. The average number of days per month with > 4 mm totals are shown at the top of each bar, and values are plotted in panel c). The error bars in panel c) denote confidence at the 95% confidence interval, determined using bootstrapping with replacement.

https://doi.org/10.5194/egusphere-2023-388
Preprint. Discussion started: 7 March 2023

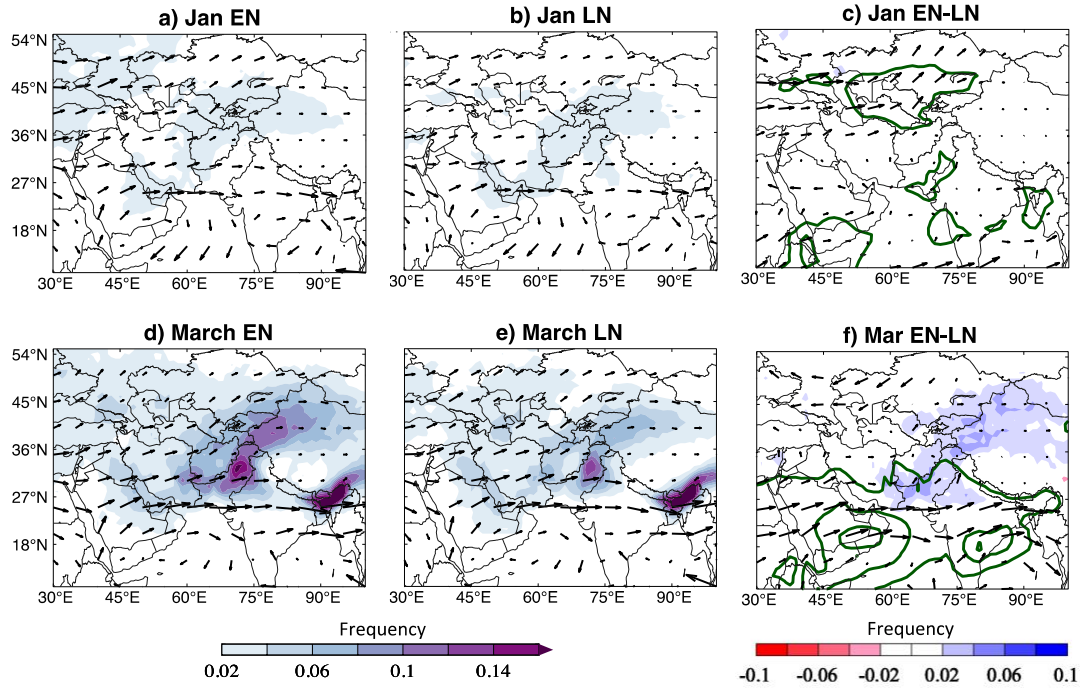

Figure 10: The color shading in a) b) d) and e) shows the mean WCB frequency (units events/6-hourly time step), and the black arrows show mean IVT, in January and March during a) El Niño and b) La Niña months. Panel c) and f) shows the January and March difference, El Niño – La Niña, respectively, while the arrows show the difference in mean IVT. The green contours in panels c) and f) show the difference in precipitable water, starting at 1 kg m^{-2} every 2 kg m^{-2}. In panels c) and f), only differences that are statistically different at the 95% confidence interval are shown.